



## OPEN ACCESS

EDITED BY  
Derek Keir,  
University of Southampton,  
United Kingdom

REVIEWED BY  
Ben Callow,  
Ghent University, Belgium  
A Barnousa,  
Taibah University, Saudi Arabia

\*CORRESPONDENCE  
Jakub Fedorik,  
✉ j.fedorik@gmail.com

SPECIALTY SECTION  
This article was submitted to  
Structural Geology and Tectonics,  
a section of the journal  
Frontiers in Earth Science

RECEIVED 17 May 2022  
ACCEPTED 20 December 2022  
PUBLISHED 10 January 2023

CITATION  
Fedorik J, Delaunay A, Losi G, Panara Y,  
Menegoni N, Afifi AM, Arkadakskiy S,  
Al Malallah M, Oelkers E, Gislason SR,  
Ahmed Z and Kunnummal N (2023),  
Structure and fracture characterization of  
the Jizan group: Implications for  
subsurface CO<sub>2</sub> basalt mineralization.  
*Front. Earth Sci.* 10:946532.  
doi: 10.3389/feart.2022.946532

COPYRIGHT  
© 2023 Fedorik, Delaunay, Losi, Panara,  
Menegoni, Afifi, Arkadakskiy, Al Malallah,  
Oelkers, Gislason, Ahmed and  
Kunnummal. This is an open-access article  
distributed under the terms of the [Creative Commons Attribution License \(CC BY\)](https://creativecommons.org/licenses/by/4.0/).  
The use, distribution or reproduction in  
other forums is permitted, provided the  
original author(s) and the copyright  
owner(s) are credited and that the original  
publication in this journal is cited, in  
accordance with accepted academic  
practice. No use, distribution or  
reproduction is permitted which does not  
comply with these terms.

# Structure and fracture characterization of the Jizan group: Implications for subsurface CO<sub>2</sub> basalt mineralization

Jakub Fedorik<sup>1\*</sup>, Antoine Delaunay<sup>1</sup>, Giacomo Losi<sup>1</sup>, Yuri Panara<sup>1,2</sup>,  
Niccolo Menegoni<sup>2</sup>, Abdulkader M. Afifi<sup>1</sup>, Serguey Arkadakskiy<sup>3</sup>,  
Murtadha Al Malallah<sup>1</sup>, Eric Oelkers<sup>4</sup>, Sigurður R. Gislason<sup>5</sup>,  
Zeyad Ahmed<sup>3</sup> and Noushad Kunnummal<sup>3</sup>

<sup>1</sup>Ali I. Al-Naimi Petroleum Engineering Research center, King Abdullah University of Science and Technology, Thuwal, Saudi Arabia, <sup>2</sup>Dipartimento di Scienze della Terra e dell'Ambiente, Università di Pavia, Pavia, Italy, <sup>3</sup>Environmental Protection, Saudi Arabian Oil Company, Dhahran, Saudi Arabia, <sup>4</sup>Géosciences Environnement Toulouse (GET), CNRS UMR 5563, Toulouse, France, <sup>5</sup>Institute of Earth Sciences, University of Iceland, Reykjavik, Iceland

The coastal region of southwest Saudi Arabia contains a thick sequence of Late Oligocene basalts in the Jizan Group, which accumulated along the continental rift that preceded the opening of the Red Sea. These basalts are targeted for the disposal of CO<sub>2</sub> emitted from industrial sources by subsurface carbon mineralization processes. The disposal potential of the Jizan Group basalts depends on having adequate permeability along fracture networks capable of conducting injected fluids away from the wellbores. The basalts in the Jizan Group generally lack primary permeability due to hydrothermal alteration, but are cross-cut by a dense network of fractures. In this paper, we describe and interpret the structural geology of the area based on field and geophysical data, and characterize the fracture development in the Jizan Group. The Jizan Group in the area comprises a bimodal suite of 30–21 Ma volcanic and volcanoclastic rocks and lacustrine sediments that accumulated in a continental rift valley similar to the East African rift. It consists predominantly of basaltic lavas that were fed by dense swarms of sheeted basalt dikes intruded parallel to the rift axis. Structurally the area is composed of half grabens bounded from the west by antithetic normal faults, and from the east by a megaflexure. Fractures in the Jizan Group were characterized by ground and aerial digital photogrammetry of outcrops. Mean P21 fracture intensities from 12 scattered meter scale outcrops are in the range 5–54 m<sup>-1</sup>, which demonstrates that the Jizan Group is highly fractured. Fracture directions are multimodal. The dominant fracture trend is 140–160 N, which is parallel to the sheeted dike swarms and normal faults, and therefore parallel to the paleo-rift axis. Additional conjugate and orthogonal fracture sets are also recognized. The presence of pervasive fracture-based permeability in the Jizan Group will facilitate the injection and mineral carbonation of carbon dioxide in the mafic volcanic rocks in this region.

## KEYWORDS

CO<sub>2</sub> storage, CarbFix, fracture permeability, antithetic faults, rift system, Red Sea

## Introduction

The *in situ* mineral carbonation of CO<sub>2</sub> in basaltic rocks is a promising technology for industrial-scale CO<sub>2</sub> emissions disposal. The efficiency of such a process was demonstrated by the CarbFix pilot project and CO<sub>2</sub> (and) H<sub>2</sub>S) sequestration facility in Iceland (Matter et al., 2016; Snæbjörnsdóttir et al., 2017; Snæbjörnsdóttir et al., 2018). The CarbFix method involves the injection of water and dissolved CO<sub>2</sub> into fresh or altered basalts, where the CO<sub>2</sub> reacts to permanently fix the carbon into carbonate minerals. A different approach to disposing CO<sub>2</sub> in basalts was also demonstrated at the Wallula pilot site in Washington, United States, where pure supercritical CO<sub>2</sub> was injected deep into the Columbia River basalts to be fixed in carbonate minerals (McGrail et al., 2014). In both cases, the basalt sequences targeted for injection had sufficient permeability to transport the injected fluids away from the wellbore and into the reactive rocks. While the massive interiors of basaltic lava flows are generally impermeable, interflow tuffs, and breccias are commonly porous and permeable. This is consistent with the studies of Fisher and Becker (1995) and Callow et al. (2018) (amongst others) who demonstrate that the permeability of fresh basalts varies widely between 1.0 and 1,000 md. Secondary processes such as hydrothermal alteration reduce the primary porosity and permeability of basalts (Fisher et al., 2014). When subjected to tectonic stress, however, basalts develop significant secondary, fracture-based permeability (Pollyea, 2015; Grab et al., 2017). The critical importance of secondary permeability to CO<sub>2</sub> disposal in basalts is emphasized at the CarbFix facility in Iceland, where injection wells target active fault zones, which act as the primary conduits for the CO<sub>2</sub>-charged fluids (Gunnarsson et al., 2018). The role of fracture permeability on supercritical CO<sub>2</sub> injection was also studied by Iding and Ringrose (2010), who evaluated the performance of the In Salah CO<sub>2</sub> conventional carbon capture and storage reservoir.

This study is part of a broader initiative to evaluate the carbonation potential of syn-rift basaltic volcanic rocks of the Oligocene to Early Miocene Jizan Group in the Red Sea coastal plain of southwestern Saudi Arabia. Oelkers et al. (2022) reviewed the geology and geochemistry of the Jizan Group basalts and evaluated the reactivity of representative samples by reaction path modelling and experimental work. Their results assess the fate of water-dissolved CO<sub>2</sub> injected in the Jizan Group basalts.

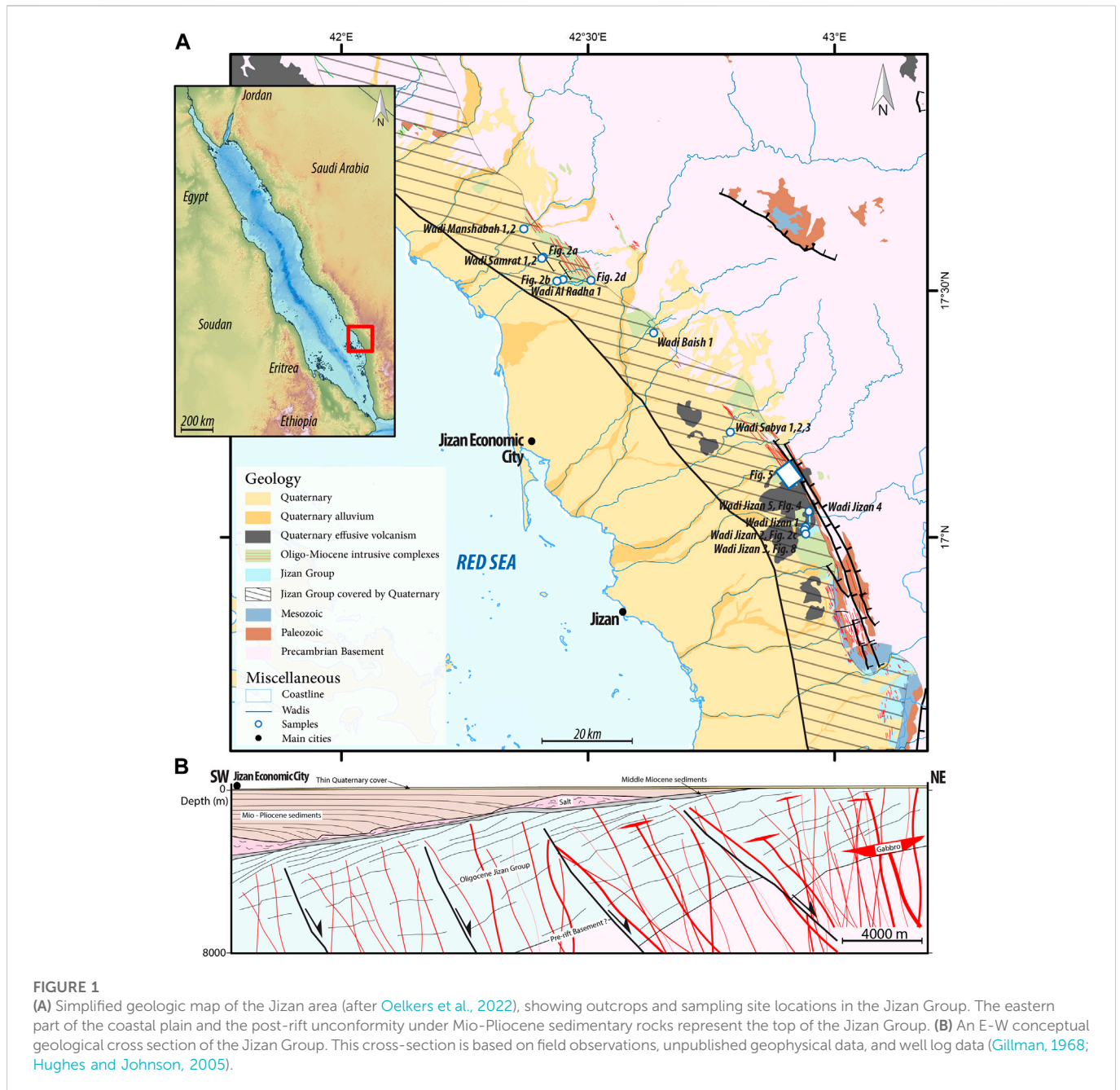
The volcanics of the Jizan Group generally lack primary permeability in vesicles, breccias, and interflow layers due to extensive hydrothermal alteration (Torres, 2020; Oelkers et al., 2022). This study focuses on quantifying the structural development of the Jizan Group volcanics in the Jizan region. First, we interpret the stratigraphic and structural setting of the Jizan Group based on new field and geophysical data. Second, we characterize fracture development in the Jizan Group using traditional outcrop studies and Terrestrial Digital Photogrammetry (TDP) and Unmanned Aerial Vehicle (UAV) Digital Photogrammetry (UAVDP). These fractures are essential to provide the permeability needed to transport injected fluids away from the wellbore allowing for their broader scale reactions with the basalt, leading to carbonate mineral precipitation in both fractures and rock matrix. This characterization provided the basis for selecting pilot well test sites and for reactive-transport modeling of the CO<sub>2</sub> reservoir by dynamic simulation of fluid injection and water-rock reactions in the subsurface.

## Geologic setting of the Jizan group

The Jizan Group was defined by Schmidt et al. (1983) as a thick sequence of mafic and felsic volcanic rocks within the Late Oligocene–Early Miocene continental rift valley that preceded the formation of the Red Sea. They informally divided the Jizan Group into several formations that proved difficult to distinguish in the field, except for the siliceous lacustrine tuffs of the Baid Formation, which contain freshwater fish, mammals, and plant fossils (Schmuff and Hadley, 1983). The age of the Jizan Group spans the interval 30–21 Ma (Late Oligocene–Early Miocene) based on fossil evidence (Madden et al., 1983) and <sup>40</sup>Ar–<sup>39</sup>Ar dating of the volcanic and subvolcanic rocks (Sebai et al., 1991; Pallister, 1987; Afifi, unpublished data). The continental rift where these rocks were deposited possibly extended from northern Somalia to the Gulf of Suez (MèGE et al., 2016). Volcanism was mostly active along the southern half of the continental rift, from Jeddah to southern Yemen, a distance of 1000 km, and it is attributed to the proximity to the Afar hotspot (Schmidt et al., 1983). Volcanism also extended further to the rift shoulders in the form of large basalt plateaus such as the Yemeni and Ethiopian flood basalts.

The Jizan Group and their lateral equivalent, the Sita Formation (Pallister, 1987), form a continuous belt of outcrops along the southern Red Sea coastal plain between latitudes 15–21 N. However, volcanic rocks are generally absent from the continental rift basins further north. Figure 1A shows the main geological features of the Jizan region. The Jizan Group volcanics consist predominantly of basaltic lava flows, tuffs, and agglomerates but also include rhyolitic ignimbrites. The volcanic and volcanoclastic lithologies are intruded by a variety of cogenetic subvolcanic rocks, which include layered gabbro lopoliths and granite stocks along the base of the volcanic sequence, and also by sheeted basalt dike swarms (i.e., Tihamat Asir dikes; Fairer, 1985; Blank and Gettings, 1985; Pallister, 1986). Several authors reported on the igneous petrology of these rocks (e.g., Schmidt et al., 1983; Coleman and McGuire, 1988; Coleman, 1993; Basch et al., 2022). Their data indicate bimodal basalt-rhyolite magmatism with few intermediate products. The volcanic rocks are extensively devitrified, hydrothermally altered and replaced by secondary assemblages, predominantly albite and chlorite, with minor prehnite, pumpellyite, epidote, zeolites, hematite, and calcite (Torres, 2020; Oelkers et al., 2022). Those mineral assemblages indicate that the volcanic rocks have been altered at temperatures as high as 300°C, likely, as suggested by Torres (2020), during the emplacement of the Tihamat Asir dikes and other intrusive rocks. This alteration has largely occluded most of the original porosity in vesicles, tuffs, and volcanoclastic sandstones of the Jizan Group rocks with secondary minerals. The Tihamat Asir dikes are less altered than the Jizan Group volcanics. About 1/3 of these are unaltered and consist of primary Ca-plagioclase (labradorite) and augite with subordinate magnetite. Altered dikes contain mostly secondary albite, chlorite and epidote. Some altered dikes also contain prehnite, zeolites (analcime, epistillbite) and calcite (Oelkers et al., 2022).

In outcrop, the Jizan Group sits unconformably over the Proterozoic basement and erosional remnants of pre-rift sedimentary rocks of Paleozoic and Mesozoic ages (i.e., the Wajid, Khums, and Amran Formations). The pre-rift sedimentary rocks and overlying Jizan Group rocks were variably tilted, on average ~30° towards the Red Sea by numerous steep and low-dipping normal faults (Voggenreiter et al., 1988; Bohannon, 1989).



The subsurface structure under the coastal plain in the area is revealed by several vintages of reflection seismic surveys acquired for hydrocarbon exploration (e.g., Gillman, 1968). The Jizan Group and subvolcanic intrusives are unconformably overlain by Miocene and younger sedimentary rocks, which include mixed-clast conglomerates, sandstones, shales, anhydrite and the Middle Miocene salts (Hughes and Johnson, 2005). The angular unconformity at the base of these sediments truncates the rift volcanics and Tihamat Asir dikes as well as all rift-related faults as revealed by geophysical data (redraw in Figure 1B). These post-rift sedimentary rocks were deposited along the newly formed passive margin of the Arabian plate and thicken to more than 4 km in the Red Sea, (Torres, 2020). The deposition of Late Miocene and younger sediments was largely controlled by salt withdrawal towards the Red Sea basin (Heaton et al., 1995).

The internal structure of the Jizan Group is generally not clear on geophysical data due to weak impedance contrasts in the lavas and scattering of seismic waves by dikes and other intrusions. However, the unpublished geophysical data (Figure 1B) reveals several seawards-tilted half grabens that are filled with layered volcanics, which display growth against antithetic NE-dipping normal faults. This suggests continuous growth of volcanic accumulation during rifting, and stepping of normal faulting from the rift margins towards the rift axis.

## Field observations

The Jizan Group outcrops as a 15 km-wide belt along the eastern part of the Red Sea shore (Figure 1A), where it was uplifted and eroded

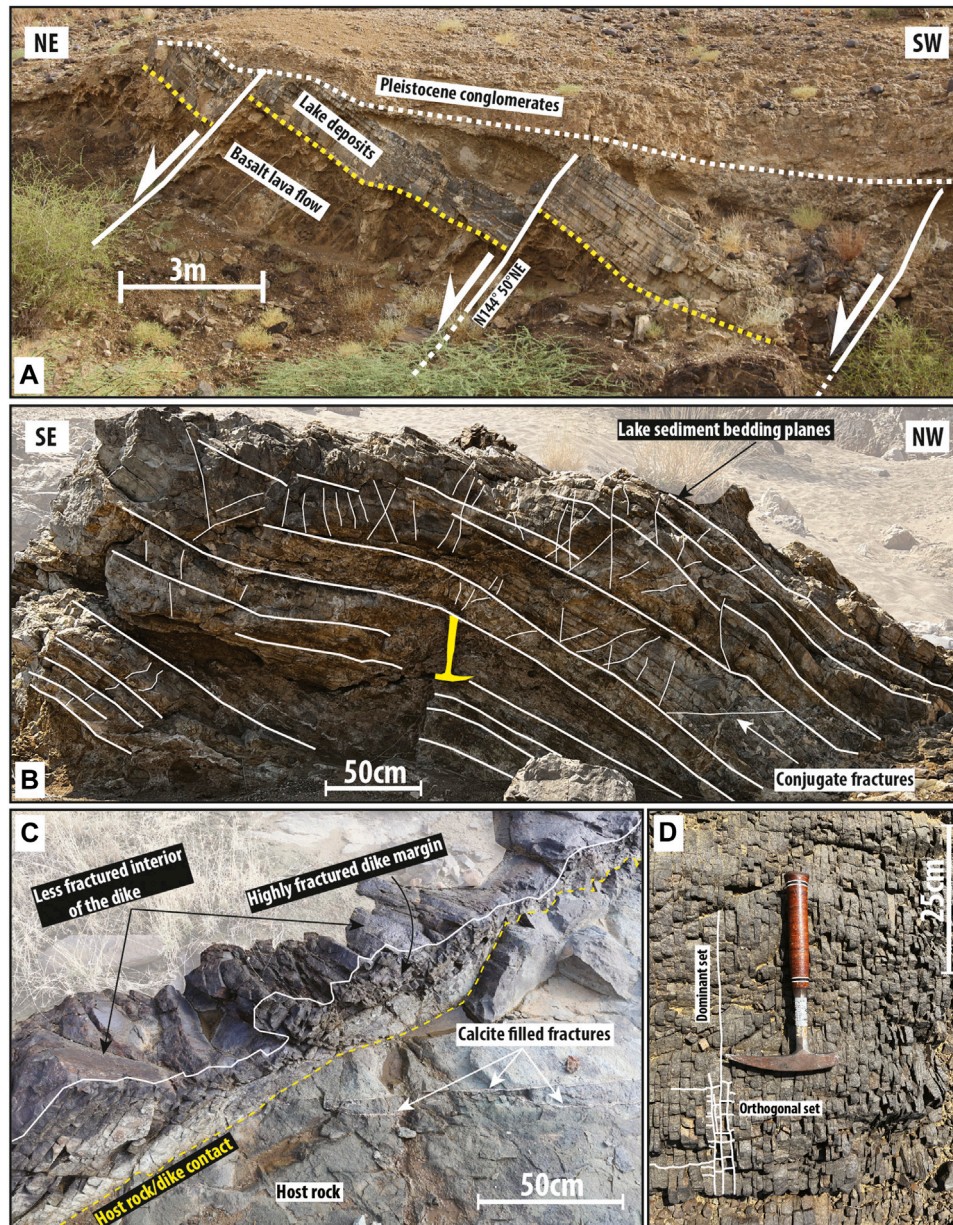


**FIGURE 2**

(A) A view towards the south of a wadi wall showing small tilt blocks separated by antithetic normal faults dipping towards the NE. Calcite precipitation is observed along the fault gouge. (B) Bent lake sediment layers associated with conjugate fractures. Calcite precipitation was observed only between the lacustrine layers. (C) Basaltic dike intruding siliceous tuffs of Jizan Group with highly fractured contact surface. (D) Orthogonal closely-spaced fracture sets in a basalt dike, the dominant set is parallel to the dike margins. See Figure 1 for locations.

flat, then covered by several meters of weakly cemented Quaternary clastic sediments. Major streams (wadis) have incised these sediments, forming shallow canyons (<20 m deep) that expose the Jizan Group along the wadi floors. The Jizan Group evidently has a soft weathering character, which is attributed to the high fracture density (Figure 2) and the hydrothermal alteration of the basalts. For fracture characterization, we focused on outcrops north, east and southeast of Jizan Economic City, which is the source of industrial CO<sub>2</sub> emissions (Figure 1A). These outcrops provide sufficient spatial coverage to determine the regional fracture pattern, which will be coupled with structural interpretation and used for future reservoir modelling.

### Structure of the Jizan group

On the high Plateau east of the Red Sea escarpment are outcrops of flat-lying Oligocene basalts (Harrat As Sirat and Harrat Hadan) that are the same age (~30 Ma) as the rift volcanics at the base of the Jizan Group. These basalts sit either over flat-lying Paleozoic or Mesozoic sedimentary rocks, or directly over the Proterozoic basement. The basalts are locally underlain by an Early Tertiary laterite that formed during the pre-rift unconformity (Schmidt et al., 1983). Although the basement, Paleozoic section, Mesozoic section, and Oligocene basalts are separated by long-lasting erosional unconformities, these unconformities are not angular and the entire succession is

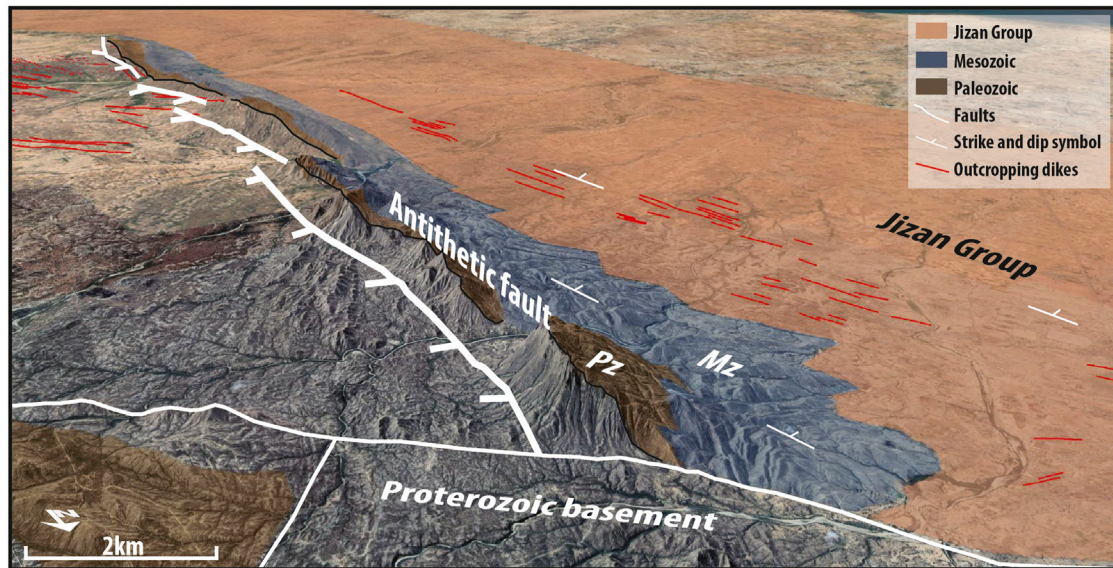


**FIGURE 3** Southward Google Earth view showing a continuous succession of Proterozoic basement, Paleozoic (Pz) and Mesozoic (Mz) sedimentary rocks and the Jizan Group. This footwall section is exhumed due to block rotation and antithetic faults. Red lines depict the location of the Tihamat Asir dike swarm in the Jizan Group (location: 16°40'46.43"N, 43°10'33.35"E).

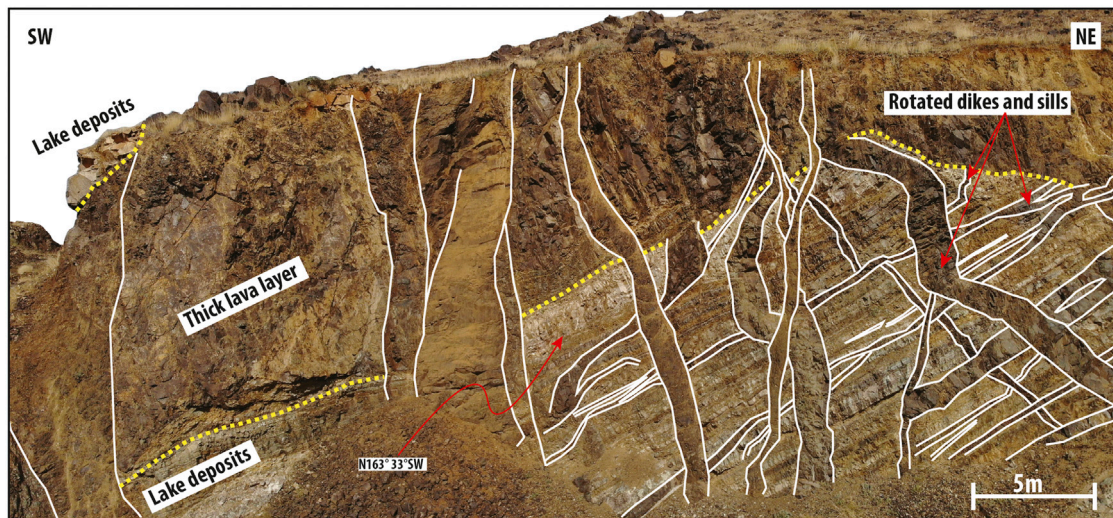


**FIGURE 4** Quarry exposing a tilt block of the Jizan Group near Wadi Jizan (outcrop location W. Jizan 5, Figure 1 and Table 2). Dashed yellow line highlights the conformable contact between basalt lava which flowed over lacustrine silicic tuffs of the Baid Formation. The volcanic sequence dips 33° towards the Red Sea in a tilted fault block. The volcanic rocks are intruded by pre- and post-tilt basalt dikes and sills (white lines).

horizontally layered. An identical stratigraphic succession is present on the Yemen and Ethiopian plateaus (e.g., Baker et al., 1996; Corti, 2009). This stratigraphic succession outcrops along the coastal plain in Jizan and Yemen, where Proterozoic basement and pre-rift sediments are consistently tilted at 30–50° towards the Red Sea (Figure 3). Previous structural studies by Bohannon (1986), Bohannon (1989) and Voggenreiter et al. (1988) established that the tilting of the pre-rift

sedimentary rocks underlying the Jizan Group is due to block rotation by antithetic (east-dipping) normal faults. The structure of the coastal plain, however, remained elusive due to poor bedrock exposure, and is addressed in the following section.

Throughout the coastal plain, the average dips in the Jizan Group are ~30° towards the Red Sea (Figures 3, 4). This is less than the 30–50 dips measured in the pre-rift section, which we attribute to block rotation by

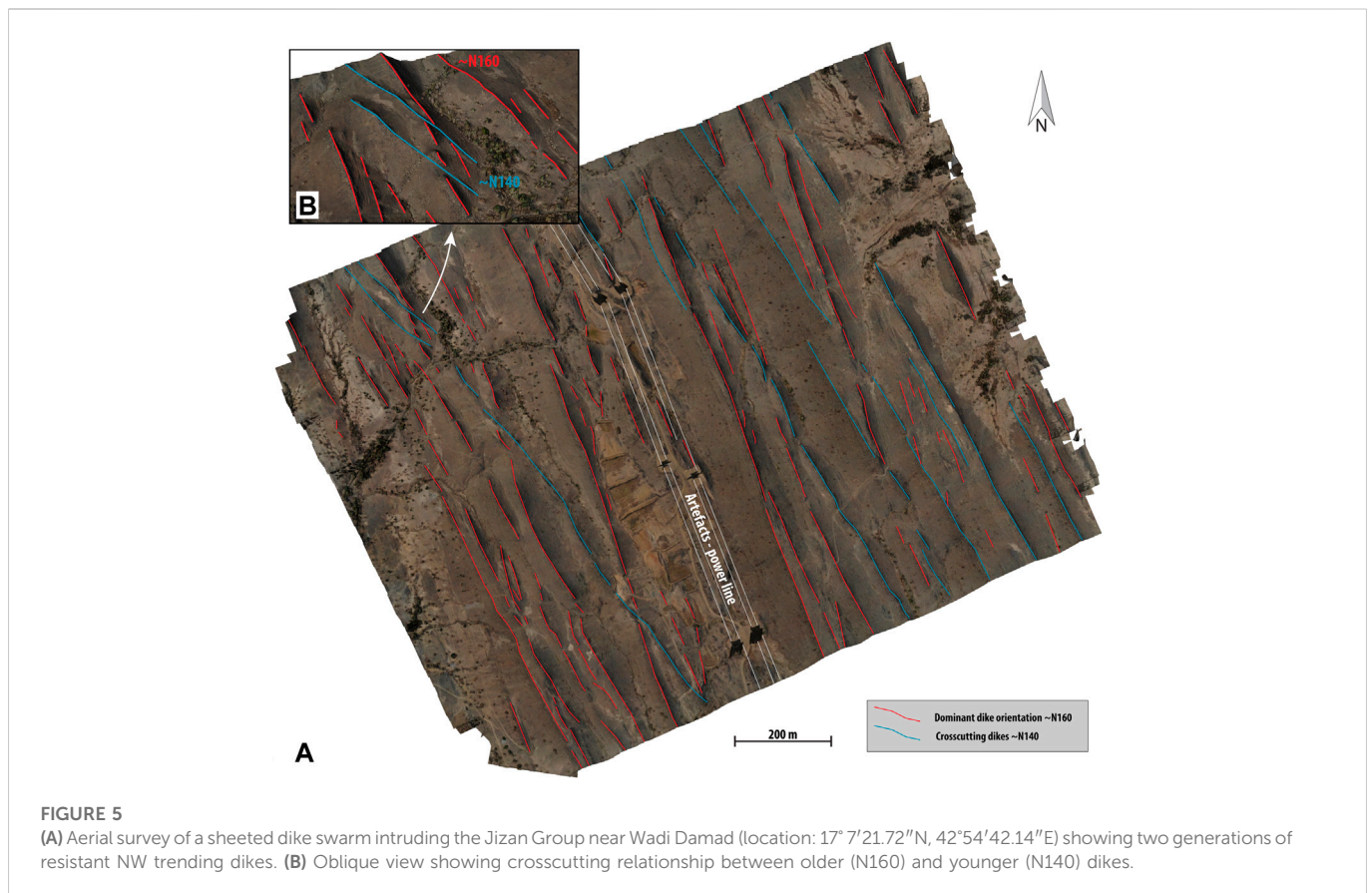


**FIGURE 5**

(A) Aerial survey of a sheeted dike swarm intruding the Jizan Group near Wadi Damad (location: 17° 7'21.72"N, 42°54'42.14"E) showing two generations of resistant NW trending dikes. (B) Oblique view showing crosscutting relationship between older (N160) and younger (N140) dikes.

antithetic normal faults during the rifting and simultaneous accumulation of the Jizan Group within half graben basins. Under the coastal plain, the presence of antithetic normal faults is confirmed by unpublished geophysical data and the redraw of a observed structures is presented in this paper (Figure 1B). We assume that the antithetic faults link at depth into a common detachment at the brittle-ductile transition in the severely necked continental crust, which is ~15 km thick underneath the coastal plain (Gettings et al., 1986).

The internal structure of the Jizan Group is generally not clear on geophysical data due to weak impedance contrasts in the lavas and scattering of seismic waves by dikes and other intrusions. However, the Jizan Group in the Ghawas area, located 300 km north of Jizan, consists of distal volcanoclastic sediments without dikes, and its internal stratigraphy is clear.

The top of the Jizan Group volcanics in the subsurface (based on unpublished geophysical data) is a coherent reflector and its depth is anchored by several well penetrations including Mansiyah-1 (Gillman, 1968; Ahmed, 1972; Hughes and Johnson, 2005). The geophysical data also indicate that the rift volcanics and rift faults were truncated during the Early Miocene by an angular unconformity, which we identify as the post-rift unconformity (Figure 1B). This unconformity dips towards the Red Sea basin ~10°, which we attribute to post-rift sag along the Arabian continental margin. The post-rift sedimentary rocks are generally unbroken by faults, except for listric faults related to salt withdrawal from the eastern margin of the continental rift. This margin appears to be a large crustal flexure in the basement (Figure 1B). The western margin of the continental rift extended, prior to continental breakup and seafloor spreading, to the Eritrean coastal plain, where Late Oligocene basalts and

lacustrine sediments of the Lower Dogali formation (Drury et al., 1994) are correlated with the Jizan Group.

A recent built quarry near Wadi Jizan (Figure 4) exposes an excellent cross section of basaltic lava flows and lacustrine silicic tuffs within the Jizan Group. This section dips 33° southwest, towards the Red Sea, and is presumably rotated against an unseen antithetic normal fault. The outcrop is intensively cross-cut by several basalt dikes and sills. The older dikes and sills are tilted while the younger dikes are subvertical. We consider observed dikes as cogenetic feeders to volcanics in the Jizan Group. The seaward tilting of the Jizan Group and feeder dikes is observed throughout the coastal plain (Figures 1B, 2A, 4).

Figure 2A shows four small tilt blocks separated by antithetic normal faults in a relatively dike free area. These faults with cemented damage zones strike NW, parallel to the sheeted basalt dikes and the trend of the Red Sea and Gulf of Suez. Figure 2B shows slightly bent layers of silicic tuff with small fractures along and across bedding (Figure 2B). The bending of a thick sequence of brittle lava and tuff layers produced this combination of conjugate fractures (Olsson et al., 2004) and flexural slip fractures (Tanner, 1989). Some calcite cemented the bedding plane fractures, but not the conjugate fractures, implying that fracture permeability was predominantly along bedding.

## Structure of the Tihamat Asir dikes and sub-volcanic plutons

A set of NW-trending basalt dikes intrude the Proterozoic basement, pre-rift sedimentary rocks, and the Jizan Group along

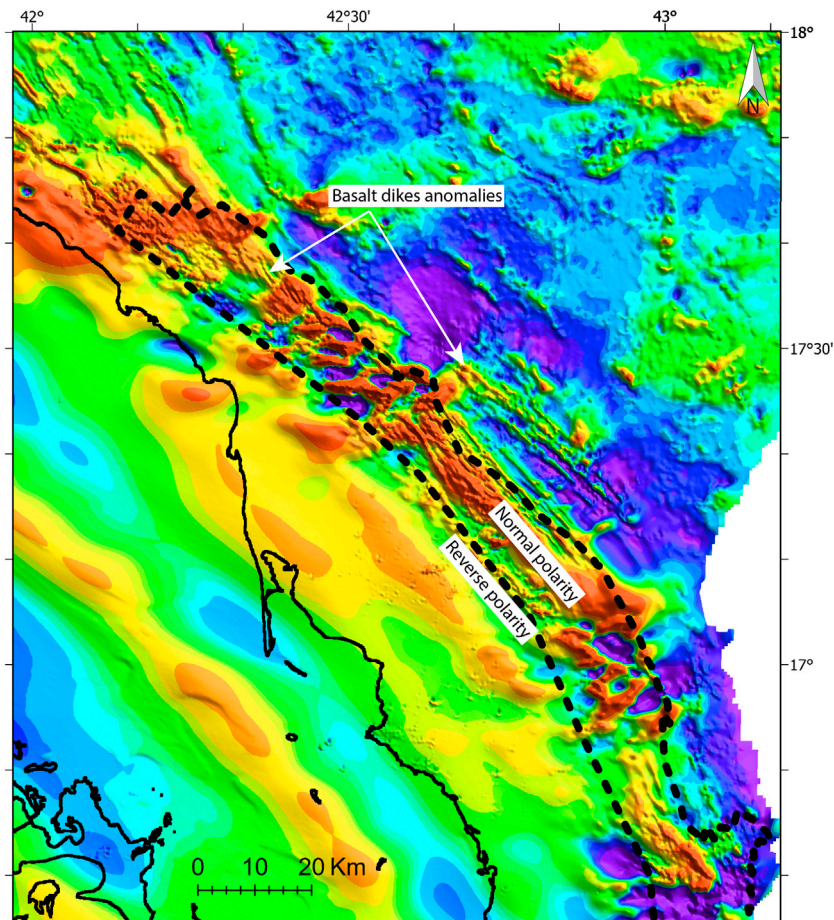


**FIGURE 6**

RTP total magnetic intensity map of the Jizan area based on data from the Saudi Geological Survey (AlMalki et al., 2014; Ibrahim et al., 2021). The dotted line delineates the ~15 km wide outcrop belt of the Jizan Group based on surface mapping (Blank and Gettings, 1985; Fairer, 1985) and interpretation of unpublished geophysical surveys. The basement and pre-rift sedimentary formations outcrop east of this belt, and the Jizan Group is unconformably covered by Mio-Pliocene sedimentary rocks west of this belt, where the amplitudes and wavelengths of magnetic anomalies are reduced. Magnetic field intensity ranges from 180 nT (red) to -120 nT (violet).

the entire eastern margin of the Red Sea, from Yemen to Sinai. These dikes are Late Oligocene to Early Miocene (30–22 Ma) in age (Steinitz et al., 1978; Feraud et al., 1991; Sebai et al., 1991; Bosworth et al., 2015). The dike swarm is particularly dense along the outcrop belt of the Jizan Group in the foothills of the Asir Escarpment (Tihamat Asir area, Basch et al., 2022), from which the name is derived. These dikes range in width from centimeters to tens of meters, and are frequently sheeted (dike in dike). They are consistently aligned to the northwest (N140–160), parallel to normal rift faults (Figure 5). Field observations also show that the vast majority of dikes are basalt/diabase, there are a few rhyolite dikes reflecting the bimodal nature of volcanism.

The basalt dikes in the Jizan Group display variable degrees of tectonic fracture development, which is primarily related to their size. Based on field observations, the larger dikes, which exceed several meters in width, are generally less fractured with higher fracture densities towards their margins (Figure 2C). In contrast, smaller dikes less than 1 m across are intensely fractured throughout. The latter display an orthogonal network of cm-spaced fractures, oriented parallel and orthogonal to the strike of the dikes (Figure 2D).

The larger basalt dikes along the outcrop belt show up prominently on aeromagnetic data as sharp linear anomalies

having mostly normal and some reverse polarities (Figure 6). These anomalies merge into broad lower amplitude anomalies under the western half of the coastal plain and offshore, where the magnetized dikes in the Jizan Group are buried under an overburden of post-rift sedimentary rocks, which thickens to ~4 km offshore. Nevertheless, the linear magnetic anomalies offshore maintain a continuous rift-parallel trend, which possibly indicates the widespread presence of dike swarms in the Jizan Group throughout the continental rift basin. Another possibility is that the broad offshore anomalies may be due to thickness variations of the Jizan Group in half graben structures.

The base of the Jizan Group is intruded by plutonic rocks of layered gabbro and granite/granophyre stocks (Figure 1A) which are described by Coleman and McGuire (1988) and Coleman and McGuire (1992). These plutonic rocks are aligned along the base of the Jizan outcrop belt (Figure 1), and according to the cross section of Coleman and McGuire (1988) are tilted by antithetic normal faults towards the Red Sea. Based on their age, structure, and location, we regard these intrusions as the shallow magma chambers which fed the volcanics of the Jizan Group.

TABLE 1 Details of the different Terrestrial Digital Photogrammetry surveys.

Outcrop name	Area (m <sup>2</sup> )	Number of images	Distance camera-outcrop (m)	Resolution (mm)	Location
W. Manshabah 1	28.6	110	2.24	0.45	N17°37'33.74"; E42°22'14.30"
W. Jizan 1	15.9	95	1.89	0.39	N17°1'24.79"; E42°56'44.75"
W. Jizan 2	24.4	47	2.46	0.52	N17°1'24.88"; E42°56'43.67"
W. Jizan 3	20.8	71	1.92	0.41	N17°1'23.84"; E42°56'45.08"
W. Jizan 4	25.8	88	1.6	0.33	N17°2'38.14"; E42°56'51.67"
W. Sabya 1	20.7	93	1.7	0.36	N17°12'52.61"; E42°47'24.26"
W. Baish 1	44.3	84	2.25	0.46	N17°24'46.22"; E42°37'57.01"
W. Al Radha 1	46.5	282	2.49	0.51	N17°31'22.29"; E42°27'12.94"
W. Samrat 1	91.4	445	2.48	0.5	N17°34'2.80"; E42°24'31.49"
W. Samrat 2	37.1	195	2.06	0.44	N17°34'2.55"; E42°24'32.16"
W. Manshabah 2	18.6	146	1.9	0.42	N17°37'31.03"; E42°22'10.87"

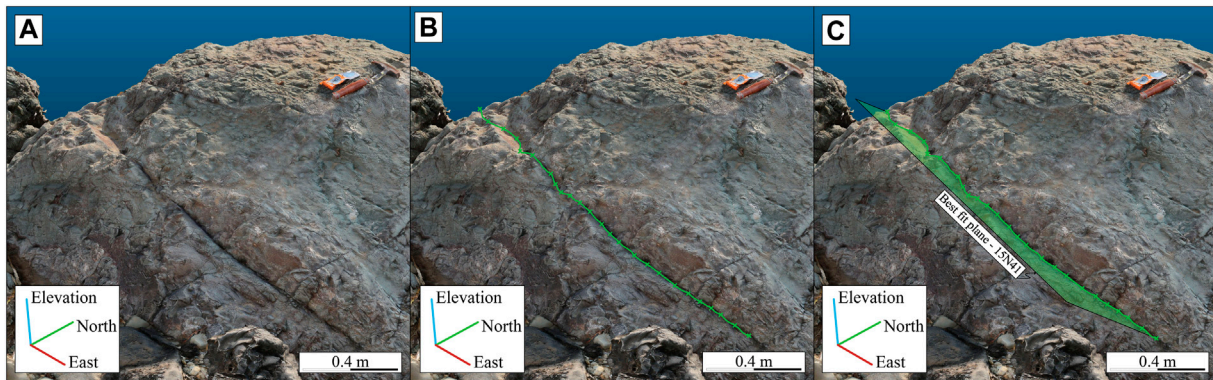


FIGURE 7

Steps of the manual fracture mapping method on 3D DOM: (A) visual inspection of the 3D model; (B) selection of the points that belong to fracture by Trace Polyline tool of Cloud Compare; (C) estimation of the best-fit plane.

## Fracture data acquisition

Due to the critical importance of fractures to providing permeability and injectivity to the basalts of the Jizan Group, the fracture networks were investigated in 14 outcrops throughout the area of interest; the location of these outcrops are shown in Figure 1A. The structural patterns observed throughout these outcrops provide a first order understanding of the regional fracture geometry and intensity at potential subsurface CO<sub>2</sub> disposal locations. To better define the results of the fracture analysis made from field observations Terrestrial Digital Photogrammetry (TDP) and Unmanned Aerial Vehicle (UAV) Digital Photogrammetry (UAVDP) have been used for acquisition of new data. The choice between TDP and UAVDP was based on the outcrop dimensions, with UAVDP used for the larger outcrops.

The TDP survey was performed using a Canon EOS 7D Mark II 20 Megapixels for 11 of the studied outcrops. The main parameters of the TDP surveys performed for each outcrop are reported in Table 1.

The 3D Digital Outcrop Models (DOMs) and 2D orthoimages were constructed using the photogrammetric Metashape (Agisoft Metashape, 2022) and all images were processed at full resolution. The 3D photogrammetric models such as shown in Figure 7, were scaled and georeferenced in a local coordinate system using a compass and hammer with known dimensions and orientation, and the corners of the compass were used as Ground Control Points (GCPs).

Manual measurements of outcrop features, such as fracture lengths and orientations, were compared with the DOM to validate the scales and orientations. In general, the scale errors are lower than 1% in length; the orientation errors are lower than 5°. These errors fall inside the range of the uncertainties of the compass-clinometer measurements (e.g., Cawood et al., 2017; Jordá Bordehore et al., 2017; Menegoni et al., 2019).

UAV photogrammetric surveys were performed using a DJI Mavic 2 enterprise quadcopter equipped with a 12-megapixel camera. Three flights were performed (Table 2) along the study area. The images were acquired keeping a UAV-outcrop distance between 7 and 16 m with an overlap always higher than 80%. The images were automatically

TABLE 2 Details of the different UAV Digital Photogrammetry surveys.

Outcrop name	Area (m <sup>2</sup> )	Number of images	Distance camera-outcrop (m)	Resolution (mm)	Location
W. Sabya 2	606	190	7	2	N17°12'46.37"; E42°47'19.92"
W. Sabya 3	374	193	6	2	N17°12'52.44"; E42°47'25.43"
W. Jizan 5	2220	628	16	5	N17°2'47.12"; E42°56'45.83"

geo-tagged and oriented using the coordinates recorded by the onboard IMU-GNSS positioning system. The parameters of the UAVDP acquisitions performed for each outcrop are reported in Table 2.

All images acquired by the UAV or by ground based camera were processed with Agisoft Metashape (version 1.6) following the procedure proposed by Menegoni et al. (2019); Inama et al. (2020). The workflow included: 1) removal of defective and blurry images (pre-processing), 2) image matching and generation of a sparse point cloud, 3) generation of colorized dense point cloud and 4) generation of topview orthoimage. This created DOM and 2D orthoimages with a resolution ranging from 5 to 21 mm.

The UAV based DOMs were georeferenced using the on-board GNSS-IMU system. This procedure allows acquisition of 3D DOM with high relative accuracy (Cawood et al., 2017) and low size and orientation errors (Menegoni et al., 2020).

## Fracture analysis

### 2D Fracture analysis

Georeferenced orthoimages were imported to QGIS using the local coordinate system for the TDP models and the WGS84-UTM38N coordinate system for the UAVDP models. These were used to map visible fractures. The fracture maps were analyzed using the FracPaQ (Healy et al., 2017) and NetworkGT (Nyberg et al., 2018) algorithms. The FracPaQ algorithm is a suite of MATLAB scripts created for the analysis of fracture orientations, dimensions, intensity, and to calculate the 2D spatial variability of the equivalent permeability ellipsoid. The NetworkGT algorithm is a QGIS plugin used to analyze the spatial variability of the fracture network connectivity, as those of the X-, Y- and I-nodes types of fracture terminations and those of the fracture branches.

### 3D Fracture analysis

The obtained 3D dense clouds and textured meshes were analyzed using CloudCompare software (CloudCompare, 2020), which allows visualization and mapping of the 3D features of the outcrops (e.g., fractures geometry; Menegoni et al., 2018; Inama et al., 2020). The 3D fracture mapping was performed using both the manual and semi-automatic sampling/tracing methods embedded in CloudCompare software. The manual method consists of manually picking the DOM points belonging to the fracture traces and/or surfaces and the estimation of the 3D planes that best-fit the point selections (Figure 7).

The semi-automatic method used in this study is based on the Compass plugin of the CloudCompare software as presented by Thiele et al. (2017). This plugin uses a least-cost path algorithm to semi-

automatically map the fracture trace based on only a few points as the start and end points of the fracture trace. These traces are then used to estimate the best-fit 3D plane.

The main advantage of the semi-automatic sampling method is the rapid measurement of the fracture traces observed over the outcrop. This method works only with the point cloud (not with textured mesh) and can map only traces. Therefore, when working with the 3D meshes or when visible fracture surfaces are present, the manual sampling procedure is used.

The fractures were mapped along their entire visible extensions to compute their orientation (dip and dip direction), position and dimensions (discontinuity length). The 3D geometrical features of fracture were exported as CSV files to perform further quantitative investigation. The dataset was analyzed with two software: Stereonet (Allmendinger et al., 2011; Cardozo and Allmendinger, 2013) and MATLAB (The Mathworks Inc., 2020), in this way it was possible to extract fracture parameters needed, as mean fracture sets dip and dip direction, dimension distribution, spatial variability and fracture frequency/intensity/density.

## Results of fracture analysis

The primary target of several field expeditions was the first order analysis of fracture orientation and intensity in the Jizan area. Fracture analysis was focused on fracture orientations and intensities. Due to poor exposure of outcrops and limited knowledge of the rotation produced by antithetic faults and/or magmatic loading, the following fracture analysis was simplified and 3D outcrops were horizontalized into orthophotos. 3D visualization was used during detailed fracture mapping on 2D orthophoto images (Figure 8).

### Fracture orientation

Figure 9 summarizes the strike of fractures at 12 scattered outcrops of the Jizan Group. In outcrops where a large number of measurements were possible (e.g., W. Sabya 2), the fracture network appears to strike in all directions, which is favorable to dispersal of injected fluids in the reservoir. However, all outcrops show at least two dominant orientations. The most dominant fracture set trends 140°–160°N, which is parallel to the continental rift axis, as inferred from the strike of normal faults (Figure 1), and from the strike of dike swarms mapped on satellite images (Figure 1), drone surveys (Figure 5) and aeromagnetic data (Figure 6). The rift-parallel fractures are extensional in origin, and some (less than 5%) are filled with secondary calcite. Most outcrops also show an orthogonal fracture set oriented roughly perpendicular to the rift-parallel fractures (Figure 2D). These orthogonal fractures are shorter and rarely

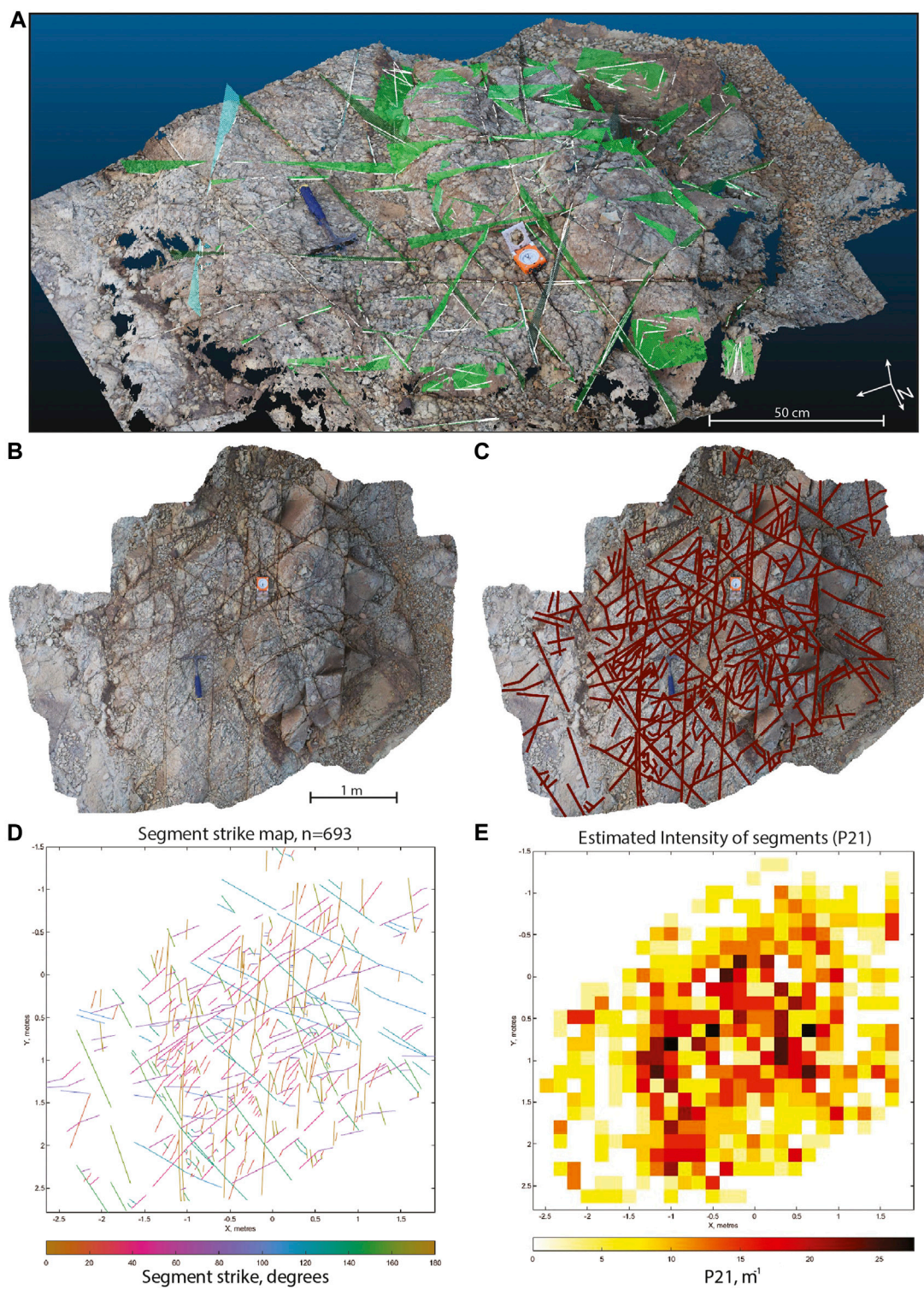


**FIGURE 8**  
 Steps of the fracture analysis of the W. Jizan 3 outcrop: **(A)** visual inspection of the 3D model; **(B)** orthophoto projection; **(C)** 2D interpretation of fractures; **(D)** fracture strike plot; **(E)** 2D fracture intensity (P21) plot. Examples of low, medium and high fracture intensity (P21) are shown in [Supplementary Figure S1](#).

crosscut the rift-parallel set. The conjugate fracture set is mapped throughout several outcrops, while only one outcrop clearly preserves such fractures and it is associated with bending of deformed layers ([Figure 2B](#)).

### Fractures intensity (P21)

The FracPaQ tool ([Healy et al., 2017](#)) was used to estimate the fracture intensity parameter P21 from the orthoimages of each outcrop. The results are

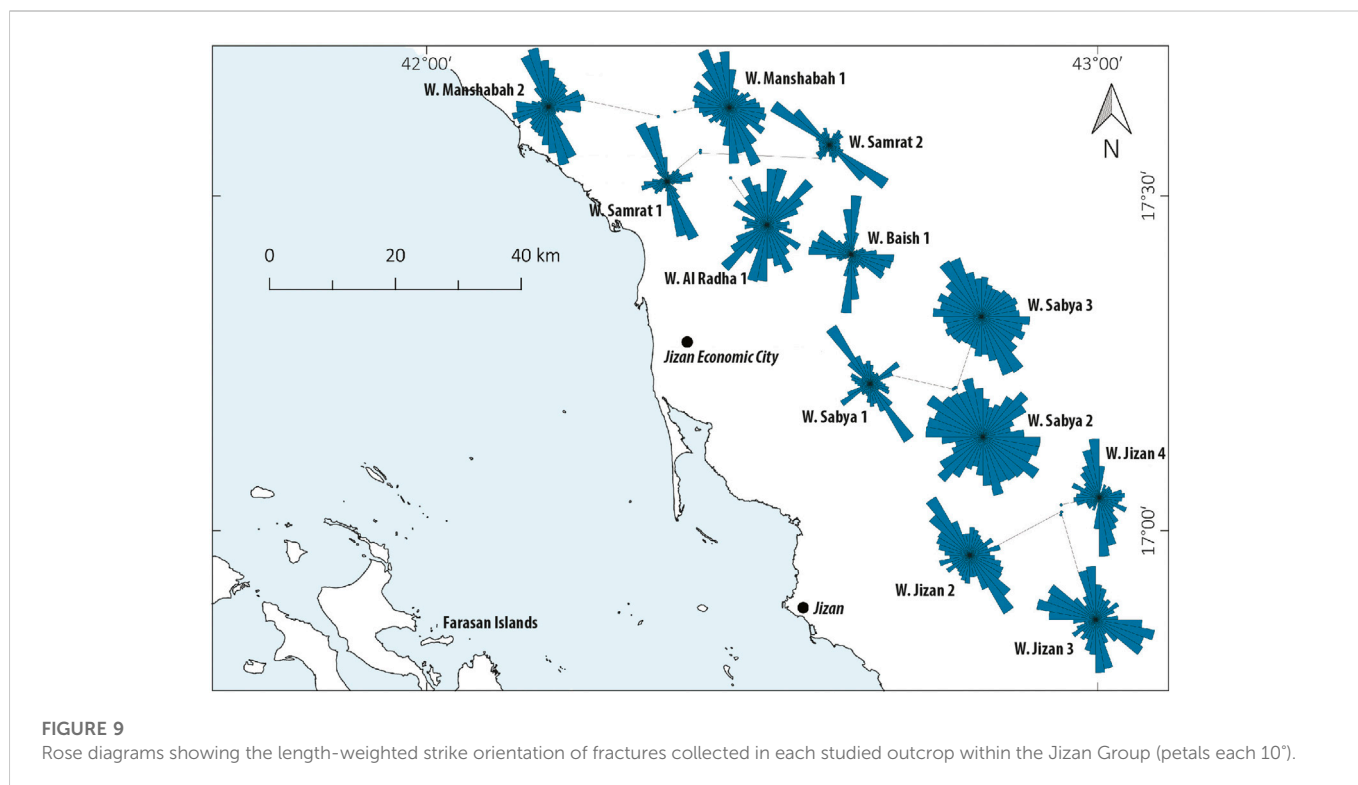


**FIGURE 9**  
Rose diagrams showing the length-weighted strike orientation of fractures collected in each studied outcrop within the Jizan Group (petals each 10°).

**TABLE 3** Statistics of the P21 analysis.

Outcrop name	P21 scan diameter (m)	P21 mean (m <sup>-1</sup> )	P21 standard deviation (m <sup>-1</sup> )	P21 maximum (m <sup>-1</sup> )
W. Manshabah 1	0.37	6.7	4.55	19.83
W. Jizan 1	0.37	5.19	3.84	25.77
W. Jizan 2	0.35	6.28	4.24	20.31
W. Jizan 3	0.33	5.58	3.13	15.58
W. Jizan 4	0.38	6.99	3.23	15.31
W. Sabya 1	0.5	4.18	2.75	12.7
W. Baish 1	0.42	3.66	2.52	14.69
W. Al Radha 1	0.37	8.96	7.57	33.71
W. Samrat 1	0.35	20.34	14.62	54.41
W. Samrat 2	0.4	12.12	7.46	29.86
W. Sabya 2	0.4	4.82	3.28	28.6
W. Sabya 3	0.4	4.61	3.48	19.15

reported in Table 3 and plotted in Figure 10. This figure presents a bubble map showing the variation of mean and maximum fracture intensity in the Jizan Group at 12 outcrops. Mean fracture intensities range from 4 to 20 m<sup>-1</sup>, and maximum fracture intensities range from 12 to 54 m<sup>-1</sup>.

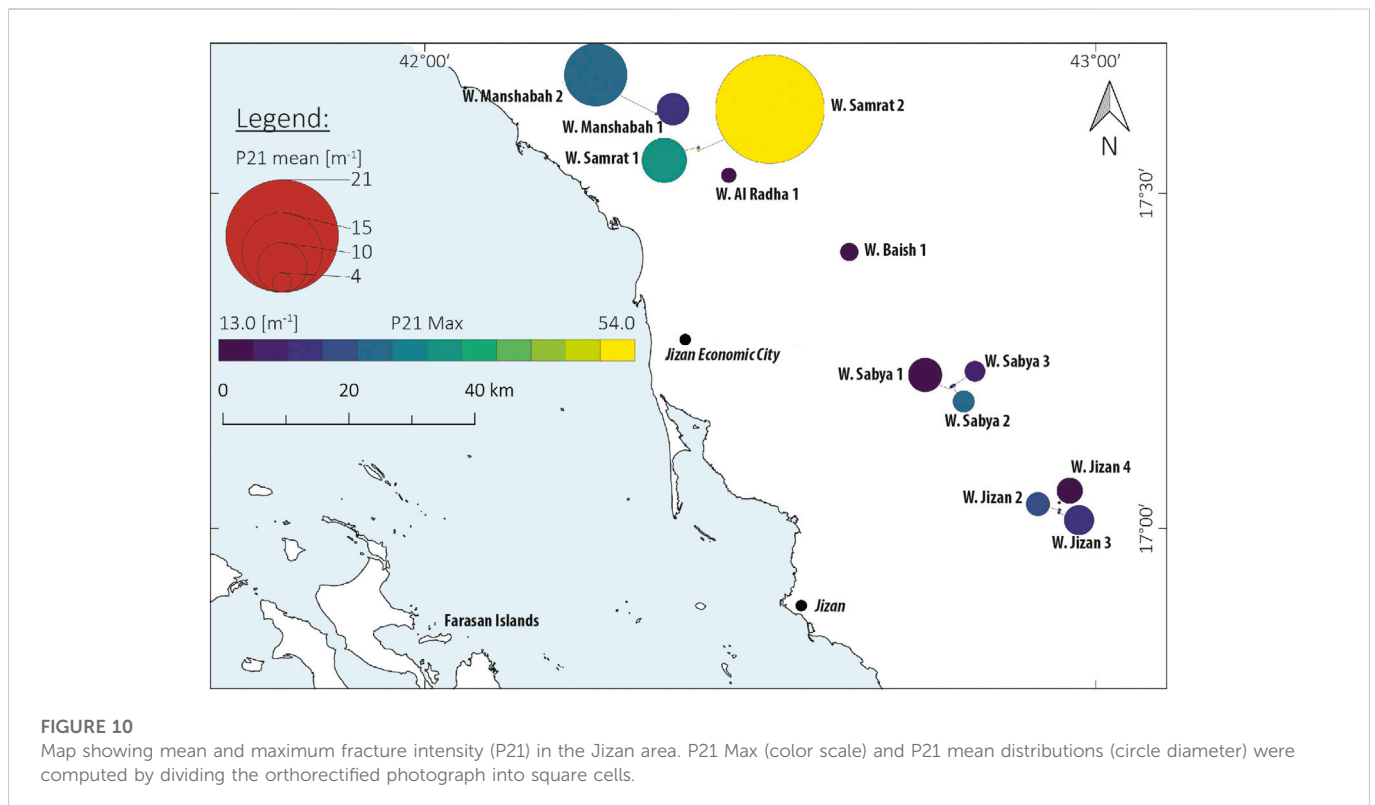
Results indicate that the Jizan Group outcrops with the highest fracture intensity are located north of Jizan Economic City. In this area, we also observed a higher proportion (up to 20%) of calcite-filled fractures, associated with the natural carbonation of the basalts by hydrothermal fluids. Nevertheless, most fractures in this area remain open indicating locally higher fracture permeability. Consequently, this general area has been selected as a target for drilling pilot wells to

confirm the subsurface properties of the Jizan Group basalts and hence their suitability to sequester CO<sub>2</sub>.

## Discussion

### Stratigraphy and structural styles in the Jizan area

Most previous workers (Almalki et al., 2015; Bosworth et al., 2005; Bosworth et al., 2020; Ligi et al., 2018; Stockli and Bosworth, 2019)



assumed that the poorly exposed Middle Miocene and younger sedimentary rocks, including the Middle Miocene salt, formed during rifting of the Red Sea. However, we emphasize that published seismic sections (Heaton et al., 1995; Tubbs et al., 2014) and unpublished geophysical surveys in Jizan area (Figure 1B) show that the deposition of these sediments was unaffected by deeply-seated normal faults, and therefore they are a post-rift sequence.

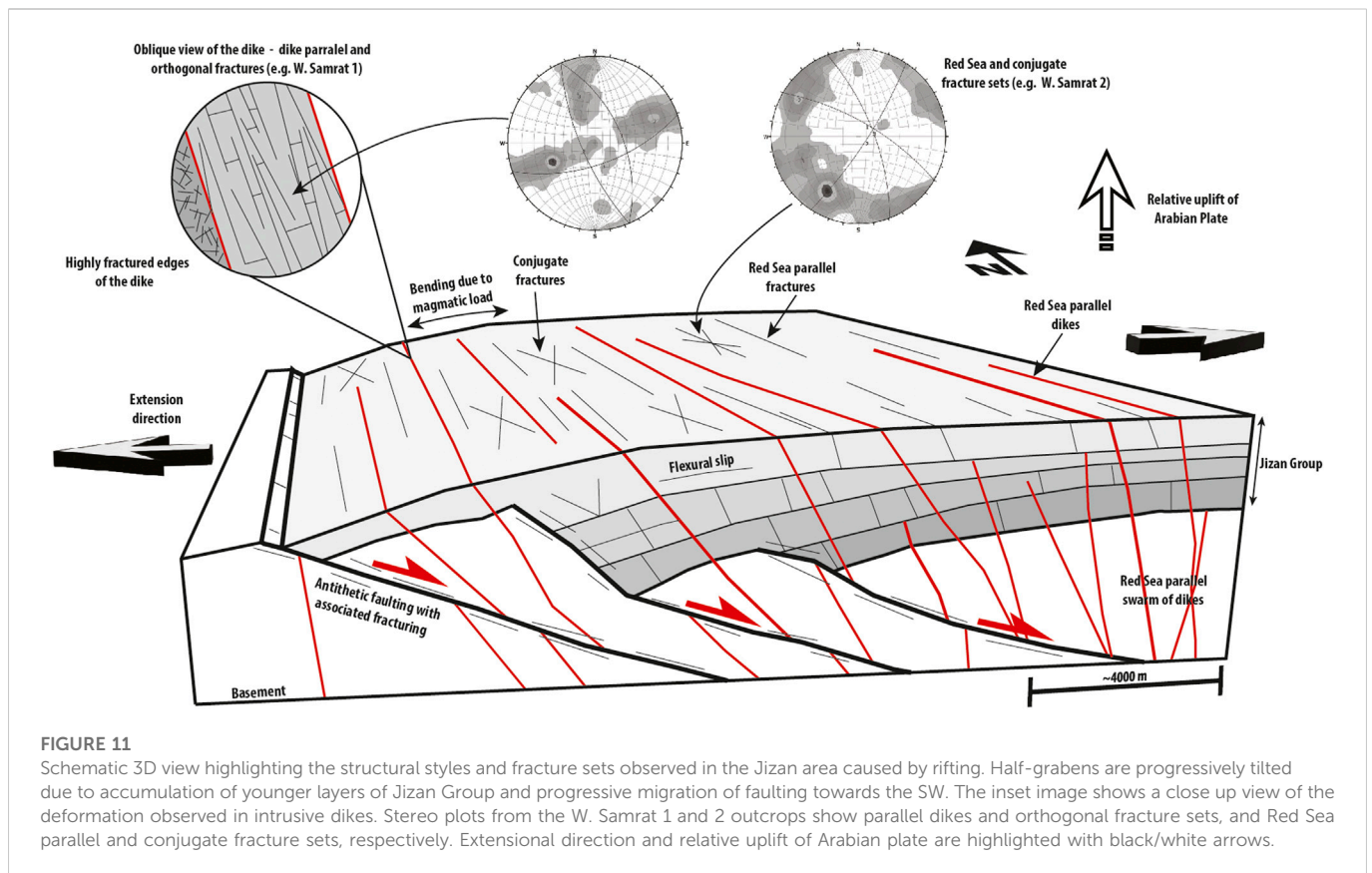
Our work based on field and geophysical (unpublished geophysical and aeromagnetic) data confirms the interpretation of Schmidt et al. (1983) that the Jizan Group formed during Oligocene continental rifting 30–22 Ma ago, and represents the entire rift sequence in the southern Red Sea. Furthermore, our interpretation of geophysical data under the coastal plain indicates that rifting in the southern Red Sea ended during the Early Miocene with a period of erosion that formed the post-rift unconformity. The Jizan Group is unconformably overlain by a post-rift sag sequence of Miocene and younger sedimentary rocks whose deposition was unaffected by rift faults.

The stratigraphy of the Jizan Group is dominated by proximal bimodal volcanism fed by swarm of sheeted dikes swarms (Tihamat Asir complex) and by shallow gabbro and granite plutons. Drone mapping reveals that the N140 set of dikes are younger as they cross-cut the older N160 dike set (Figure 5). Volcanism was not confined in the rift valley, but extended to the rift margins in Saudi Arabia, Yemen and Ethiopia, due to proximity to the Afar hotspot. However, the paleo-rift valley contained a thick accumulation of confined fluvial and lacustrine volcanoclastic rocks, along with lavas and pyroclastic rocks. The thickness of the Jizan Group is difficult to estimate due to poor seismic resolution, structural complexity, and post-rift erosion. The preserved thickness of the Jizan group is estimated to

range from zero along the eastern limit of the outcrop belt to a few kilometers toward the hanging walls of large normal faults. The structure of the basement, pre-rift sedimentary rocks, and the Jizan Group is dominated by antithetic normal rift faults, which rotated these blocks towards the Red Sea (Figure 1B).

Large scale geomorphological observations show non-symmetrical rifting as the shoulder of the Arabian plate rift is at a higher elevation than the rift shoulder of the Nubian plate. Similar non-symmetry is observed along the strike of the Red Sea, as the elevation of the Red Sea Escarpment increases continuously towards the southeast. The vertical change observed in the Jizan area is, therefore, the highest along the Saudi Red Sea coast. The Western Afar Margin also shows a significant relative elevation change between the Ethiopian Plateau and the marginal area of the Afar Depression (equivalent to the Jizan area). This margin is deformed with antithetic faults similar to those observed in the Jizan area. According to Wolfenden et al. (2005), Corti et al. (2015) and Zwaan et al. (2020) the flexure model, which combines relative vertical movement, extension and magmatic loading, is capable of forming antithetic faults and rotated blocks such as observed in the Jizan area.

Although Jizan Group exposure at surface is limited, block rotation towards the Red Sea is indicated by tilted lava flows, lake beds, and intruding dikes and sills. These observations provide evidence for the presence of antithetic faults below the surface. Indeed, geophysical data from the area confirm the presence of antithetic faults in the subsurface (Figure 1B). These unpublished data also reveals that the top layers of the Jizan Group grew against the antithetic faults and deformation propagated towards the southwest. Only the upper part of the Jizan Group can be imaged likely due to prominent diking, which decreases the resolution of the seismic image deeper in the section. Important loading due to magmatic



accumulation and migration of fault activity towards the Red Sea could be the cause of the bending of the Jizan Group.

### Fracture types

The dominant fracture set, as observed in all Jizan Group outcrops, has a strike, that is, parallel to the Red Sea (140°–160°N). These Mode-I fractures are perpendicular to the least, and parallel to the maximum and intermediate, compressive stress axes (e.g., Smith, 1997). Extension fractures can also accommodate dikes (Peacock et al., 2016), which we also observe in the field, where the dike swarm has the same strike orientation as the dominant fracture set.

Conjugate fractures represent the second most common fractures observed in the field and we find these in several outcrops throughout the study area. Such fractures are not common in extensional domains, but are present in several outcrops in various locations in the study area. Conjugate fractures are often associated with folding and they form in the hinge zones of folds (Cosgrove, 2015). We do not anticipate compressional structures in the Jizan area, however, magmatic loading and the migration of faulting towards the Red Sea bends the juxtaposed layers. According to McDermott et al. (2018), lithosphere cooling increases the subcrustal load acting on the plate and, as a consequence, bends it downward. Bending of the Jizan Group associated with conjugate fractures and faulting was observed in both the field and in geophysical data (Figures 1B, 2B). Davatzes and Aydin (2003) reported conjugate faulting and bending caused by an extensional tectonic system. This bending accounts for

the high density of bed parallel and oblique conjugate fractures in the Jizan Group.

One additional apparent fracture set observed in the field and during the photogrammetry analysis is orthogonal to the dominant Red Sea fracture set. This fracture set is observed only inside larger dikes, which are predominantly oriented parallel to the Red Sea (Figure 2D). In general, the entire Jizan Group is highly fractured due to the brittle nature of lava and siliceous tuff layers. Most fractures observed at surface have clearly developed within a syn-tectonic activity (Figure 11), and provide encouraging preliminary information about fracture sets expected in the subsurface. However, further studies focusing on subsurface fracture orientation, aperture or roughness must be performed. Furthermore, the extent of widespread hydrothermal alteration in the volcanic/subvolcanic rocks seems proportional to fracture intensity.

### Potential for mineral storage in the Jizan group

Key to the successful mineral storage in basaltic rocks is the ability to inject substantial quantities of fluid into the reactive rock reservoir, and for the injected fluids to encounter substantial reactive mineral surface areas along their flow paths. As hydrothermal alteration tends to fill the primary porosity of basaltic rocks, development of secondary fracture porosity and permeability in the prospective reactive rock reservoirs becomes essential. The results of this study reveal the existence of a large number of intersecting fractures in the Jizan Group basalts. The cross-cutting distribution of the fracture network is

expected to enhance the transmission of injected fluids throughout the volcanics. Most fractures have clean surfaces with no evidence of alteration and/or mineral precipitation. This indicates that those fractures remain open to fluid flow and the exposed rock surfaces remain reactive for the promotion of subsurface carbonation reactions.

The results of this study reveal several favorable targets for CO<sub>2</sub> injection into the Jizan Group. Notably the geophysical data (Figure 1B) indicate the existence of important antithetic faults with offsets of several hundreds of meters. Such faults can have important damage zones of very high permeability (Fossen and Bale, 2007). These structures could, therefore, be targeted as primary injection zones. In addition, fracture intensity (Figure 10) analysis confirms the existence of very high fracturing across the entire Jizan Group. Even considering that digital photogrammetric resolution is affected by the used methodology (Nex and Remondino, 2014) and by the scale of the investigation (Bossennec et al., 2021) the fracture intensity values observed in the study area are remarkable compared with other P21 values (e.g. Elmo and Stead, 2010; Watkins et al., 2015; Ceccato et al., 2021). Such high degree of fracturing is not observed in flat lying volcanic layers in other volcanic fields in Saudi Arabia. Outcrops north of Jizan Economic City exhibit the highest fracture intensity, therefore, this area may hold the greatest potential for injecting and sequestering CO<sub>2</sub>.

The presence of prominent dike swarms in the area (Figures 5, 6) is expected to have important implications for the direction of fluid flow in the subsurface. Even though some dikes are fractured, the central sections of others are massive and therefore less likely to transmit fluids (Figure 2C). The existence of such linear, low-permeability features suggests that the dominant direction of fluid flow in the subsurface will likely be NW-SE. At the same time, the higher degree of fracturing along the contacts of most dikes is expected to facilitate fluid flow and to also provide mineral-fluid surface areas for mineral carbonation.

The combination of field, well and geophysical data reveal that the top of the Jizan Group is covered by a thin layer of Quaternary sediments in the northeastern half of the coastal plain. The basalts are increasingly buried to west, as the entire Jizan Group dips ~10° towards the Red Sea such that at the coast the top of this group is beneath ~4 km of sediments (Gillman, 1968; Hughes and Johnson, 2005). The thickness of the basalts was estimated to most likely be 1 km, with a minimum and maximum thickness ranging from 0.3 to 1.5 km (Oelkers et al., 2022). This study demonstrates that the thickness of the Jizan Group against major antithetic faults is expected to increase towards the Red Sea.

The increasing depth of the Jizan group to the west allows for choosing optimal CO<sub>2</sub> disposal sites in the region. The most rapid carbonation of basaltic rocks occurs likely within the 100°C–200°C temperature range (Kelemen and Matter, 2008; Clark, et al., 2020; Marieni et al., 2021). The injection of CO<sub>2</sub> as a dissolved aqueous phase is favored at pressures greater than 25 bars, while the injection of supercritical CO<sub>2</sub> requires pressures in excess of 80 bars (Gislason et al., 2010; Vilarasa et al., 2013; Snæbjörnsdóttir et al., 2020). Therefore, the increasing depth of the Jizan Group provides the opportunity to locate injection sites targeting reservoir domains where subsurface pressure and temperature conditions are optimal for CO<sub>2</sub> disposal by both mineral carbonation and potentially by supercritical CO<sub>2</sub> injection.

## Conclusion

This study of the structural styles, fracturing and the potential fluid flow paths in the Jizan Group basalts suggest that ample fracture permeability and mineral-fluid surface area is available for the injection and mineralization of CO<sub>2</sub> in the subsurface. Notably, three principal interconnected fracture sets are evident in these rocks. The fracturing intensity of these rocks is high, having mean P21 approximately 6 m<sup>-1</sup>, while the most fractured area was observed north of Jizan Economic City with P21 mean reaching 20 m<sup>-1</sup>. The lateral extent and presence of the similar fracture sets across several tens of kms, indicates that these fracture sets are also present at depth. In general, the entire Jizan Group is highly fractured due to the brittle nature of the lava and siliceous tuff layers in the sequence. This is supported by field observations and the interpretation of aeromagnetic and geophysical data. Evidence for the presence of tilted blocks, antithetic faults, and significant magmatic accumulations confirms the flexural model for the Jizan area. Structurally, the Jizan Group is filling a set of half grabens bounded from the west by antithetic normal faults with fault activity migration towards the Red Sea. Consequently, the results of this study support the CO<sub>2</sub> storage capacity estimates suggesting that the basaltic rocks of the Jizan region have the capacity to store from 140 to 1000 years of CO<sub>2</sub> emissions generated from the Jizan Economic City as stable carbonate minerals (Oelkers et al., 2022). Similar tectono-volcanic conditions are expected to continue for about 500 km further north along the Red Sea shore, which underscores the potential of Jizan Group as one of the principal CO<sub>2</sub> sinks that can help fulfil the decarbonization aspirations of the Kingdom of Saudi Arabia.

## Data availability statement

The original contributions presented in the study are included in the article/Supplementary Material, further inquiries can be directed to the corresponding author.

## Author contributions

JF, concept, seismic, fieldwork, structural, and fracture analysis, figures, and writing; AD, fieldwork, figures, and writing; GL, photogrammetry, fracture analysis, writing; YP, photogrammetry, fracture analysis, figures and writing; NM, photogrammetry, fracture analysis, writing; AA, primary advisor, regional geology, figures, and writing; SA, seismic, regional geology, fieldwork, writing; MM, fieldwork, fracture analysis, writing; EO, CO<sub>2</sub> mineralisation, fieldwork, writing; SG, CO<sub>2</sub> mineralisation, fieldwork, writing; ZA, CO<sub>2</sub> mineralisation, fieldwork, writing; NK, CO<sub>2</sub> mineralisation, writing.

## Funding

This research was supported with two fundings: Saudi aramco research grant nb. 4480 and baseline of AA, nb. 1400/01/01.

## Conflict of interest

The authors declare that the research was conducted in the absence of any commercial or financial relationships that could be construed as a potential conflict of interest.

## Publisher's note

All claims expressed in this article are solely those of the authors and do not necessarily represent those of their affiliated organizations, or those of the publisher, the editors and the reviewers. Any product that may be evaluated in this article, or

claim that may be made by its manufacturer, is not guaranteed or endorsed by the publisher.

## Supplementary material

The Supplementary Material for this article can be found online at: <https://www.frontiersin.org/articles/10.3389/feart.2022.946532/full#supplementary-material>

### SUPPLEMENTARY FIGURE S1

Interpreted orthoimage, intensity P21 plot and strike map of three different outcrops showing high (W. Manshabah 2), average (W. Sabya 1) and low (W. Jizan 3) P21 fracture intensity.

## References

- Agisoft Metashape (2022). *Agisoft Metashape [Commercial software]*. St. Petersburg, Russia: Agisoft LLC. Available at: <https://www.agisoft.com/> (Accessed January 1, 2022).
- Ahmed, S. S. (1972). Geology and petroleum prospects in Red Sea. *AAPG Bull.* 56 (4), 707–719. doi:10.10136/818A407A-16C5-11D7-8645000102C1865D
- Allmendinger, R. W., Cardozo, N., and Fisher, D. M. (2011). *Structural geology algorithms: Vectors and tensors*. Cambridge: Cambridge University Press.
- Almalki, K. A., Betts, P. G., and Ailleres, L. (2014). Episodic sea-floor spreading in the southern Red Sea. *Tectonophysics* 617, 140–149. doi:10.1016/j.tecto.2014.01.030
- Almalki, K. A., Betts, P. G., and Ailleres, L. (2015). The Red Sea–50 years of geological and geophysical research. *Earth-Science Rev.* 147, 109–140. doi:10.1016/j.earscirev.2015.05.002
- Baker, H. R., Jr, and Gettings, M. E. (1996). A brief Oligocene period of flood volcanism in Yemen: Implications for the duration and rate of continental flood volcanism at the afro-arabian triple junction. *Earth Planet. Sci. Lett.* 138, 39–55. doi:10.1016/0012-821x(95)00229-6
- Basch, V., Sanfilippo, A., Vigliotti, L., Langone, A., Rasul, N., Khorsheed, M., et al. (2022). Crustal contamination and hybridization of an embryonic oceanic crust during the Red Sea rifting (Tihama Asir igneous complex, Saudi Arabia). *J. Petrology* 63, egac005. doi:10.1093/ptrology/egac005
- Blank, H. R., Jr, and Gettings, M. E. (1985). *Reconnaissance geologic map of the jizan quadrangle, sheet 16/42 B, kingdom of Saudi Arabia*. USA: US Geological Survey.
- Bohannon, R. G. (1986). Tectonic configuration of the Western Arabian continental margin, southern Red Sea. *Tectonics* 5, 477–499. doi:10.1029/tc005i004p00477
- Bohannon, R. (1989). Style of extensional tectonism during rifting, Red Sea and gulf of aden. *J. Afr. Earth Sci. (and the Middle East)* 8, 589–602. doi:10.1016/s0899-5362(89)80046-6
- Bossennec, C., Frey, M., Seib, L., Bär, K., and Sass, I. (2021). Multiscale characterisation of fracture patterns of a crystalline reservoir analogue. *Geosciences* 11, 371. doi:10.3390/geosciences11090371
- Bosworth, W., Huchon, P., and Mcclay, K. (2005). The red sea and gulf of aden basins. *Journal of African Earth Sciences* 43, 334–378. doi:10.1016/j.jafrearsci.2005.07.020
- Bosworth, W., Khalil, S., Ligi, M., Stockli, D., and Mcclay, K. (2020). “Geology of Egypt: The northern Red Sea,” in *The geology of Egypt* (Germany: Springer), 343–374.
- Bosworth, W., Stockli, D. F., and Helgeson, D. E. (2015). Integrated outcrop, 3D seismic, and geochronologic interpretation of Red Sea dike-related deformation in the Western Desert, Egypt—the role of the 23 Ma Cairo “mini-plume”. *Journal of African Earth Sciences* 109, 107–119. doi:10.1016/j.jafrearsci.2015.05.005
- Callow, B., Falcon-Suarez, I., Ahmed, S., and Matter, J. (2018). Assessing the carbon sequestration potential of basalt using X-ray micro-CT and rock mechanics. *International Journal of Greenhouse Gas Control* 70, 146–156. doi:10.1016/j.ijggc.2017.12.008
- Cardozo, N., and Allmendinger, R. W. (2013). Spherical projections with OSX Stereonet. *Computers & Geosciences* 51, 193–205. doi:10.1016/j.cageo.2012.07.021
- Cawood, A. J., Bond, C. E., Howell, J. A., Butler, R. W., and Totake, Y. (2017). LiDAR, UAV or compass-clinometer? Accuracy, coverage and the effects on structural models. *Journal of Structural Geology* 98, 67–82. doi:10.1016/j.jsg.2017.04.004
- Ceccato, A., Viola, G., Antonellini, M., Tartaglia, G., and Ryan, E. J. (2021). Constraints upon fault zone properties by combined structural analysis of virtual outcrop models and discrete fracture network modelling. *Journal of Structural Geology* 152, 104444. doi:10.1016/j.jsg.2021.104444
- Clark, D. E., Oelkers, E. H., Gunnarsson, I., Sigfússon, B., Snæbjörnsdóttir, S. Ó., Aradóttir, E. S., et al. (2020). CarbFix2: CO<sub>2</sub> and H<sub>2</sub>S mineralization during 3.5 years of continuous injection into basaltic rocks at more than 250° C. *Geochimica et Cosmochimica Acta* 279, 45–66. doi:10.1016/j.gca.2020.03.039
- CloudCompare [GPL software] (2022). *Cloud compare open source project*. Available at: <http://www.cloudcompare.org/> (Accessed January 1, 2022).
- Coleman, R. G. (1993). “Geological evolution of the Red Sea,” in *Oxford monographs on geology and geophysics* (New York: Oxford University Press).
- Coleman, R. G., and Mcguire, A. V. (1988). Magma systems related to the Red Sea opening. *Tectonophysics* 150, 77–100. doi:10.1016/0040-1951(88)90296-x
- Corti, G., Agostini, A., Keir, D., Van Wijk, J., Bastow, I. D., and Ranalli, G. (2015). Magma-induced axial subsidence during final-stage rifting: Implications for the development of seaward-dipping reflectors. *Geosphere* 11, 563–571. doi:10.1130/ges01076.1
- Corti, G. (2009). Continental rift evolution: From rift initiation to incipient break-up in the main Ethiopian rift, east africa. *Earth-Science Reviews* 96, 1–53. doi:10.1016/j.earscirev.2009.06.005
- Cosgrove, J. (2015). The association of folds and fractures and the link between folding, fracturing and fluid flow during the evolution of a fold–thrust belt: A brief review. *Geological Society, London, Special Publications* 421, 41–68. doi:10.1144/sp421.11
- Davatzes, N. C., and Aydin, A. (2003). The formation of conjugate normal fault systems in folded sandstone by sequential jointing and shearing, Waterpocket monocline, Utah. *Journal of Geophysical Research Solid Earth* 108, 1795–1813. doi:10.1016/S0191-8141(03)00043-9
- Drury, S., Kelley, S., Berhe, S., Collier, R. L., and Abraha, M. (1994). Structures related to Red Sea evolution in northern Eritrea. *Tectonics* 13, 1371–1380. doi:10.1029/94tc01990
- Elmo, D., and Stead, D. (2010). An integrated numerical modelling–discrete fracture network approach applied to the characterisation of rock mass strength of naturally fractured pillars. *Rock Mechanics and Rock Engineering* 43, 3–19. doi:10.1007/s00603-009-0027-3
- Fairer, G. (1985). Evolution of the asir terrane and Phanerozoic rifting in southwestern Saudi Arabia. *Geol. Soc. Am. 17*. Abstr. Programs;(United States).
- Féraud, G., Zumbo, V., Sebai, A., and Bertrand, H. (1991). 40Ar/39Ar age and duration of tholeiitic magmatism related to the early opening of the Red Sea rift. *Geophysical Research Letters* 18, 195–198. doi:10.1029/91gl00207
- Fisher, A. T., Alt, J., and Bach, W. (2014). “Chapter 4.2.2 - hydrogeologic properties, processes, and alteration in the igneous ocean crust,” in *Developments in marine geology*. Editors R. Stein, D. K. Blackman, F. Inagaki, and H.-C. Larsen (Netherlands: Elsevier), 507–551.
- Fisher, A. T., and Becker, K. (1995). Correlation between seafloor heat flow and basement relief: Observational and numerical examples and implications for upper crustal permeability. *Journal of Geophysical Research Solid Earth* 100, 12641–12657. doi:10.1029/95jb00315
- Fossen, H., and Bale, A. (2007). Deformation bands and their influence on fluid flow. *AAPG bulletin* 91, 1685–1700. doi:10.1306/07300706146
- Gettings, M. E., Blank, H., Jr, Mooney, W., and Healey, J. (1986). Crustal structure of southwestern Saudi Arabia. *Journal of Geophysical Research Solid Earth* 91, 6491–6512. doi:10.1029/jb091i10p06491
- Gillman, M. (1968). “Primary results of a geological and geophysical reconnaissance of the Jizan coastal plain in Saudi Arabia,” Regional Technical Symposium, Saudi Arabia, March 27–29, 1968.
- Gislason, S. R., Wolff-Boenisch, D., Stefansson, A., Oelkers, E. H., Gunnlaugsson, E., Sigurdardóttir, H., et al. (2010). Mineral sequestration of carbon dioxide in basalt: A pre-injection overview of the CarbFix project. *International Journal of Greenhouse Gas Control* 4, 537–545. doi:10.1016/j.ijggc.2009.11.013
- Grab, M., Quintal, B., Caspari, E., Maurer, H., and Greenhalgh, S. (2017). Numerical modeling of fluid effects on seismic properties of fractured magmatic geothermal reservoirs. *Solid Earth* 8, 255–279. doi:10.5194/se-8-255-2017

- Gunnarsson, I., Aradóttir, E. S., Oelkers, E. H., Clark, D. E., Arnarson, M. P., Sigfússon, B., et al. (2018). The rapid and cost-effective capture and subsurface mineral storage of carbon and sulfur at the CarbFix2 site. *International Journal of Greenhouse Gas Control* 79, 117–126. doi:10.1016/j.ijggc.2018.08.014
- Healy, D., Rizzo, R. E., Cornwell, D. G., Farrell, N. J., Watkins, H., Timms, N. E., et al. (2017). FracPaQ: A MATLAB™ toolbox for the quantification of fracture patterns. *Journal of Structural Geology* 95, 1–16. doi:10.1016/j.jsg.2016.12.003
- Heaton, R., Jackson, M., Bamahmoud, M., and Nani, A. (1995). *Superposed Neogene extension, contraction, and salt canopy emplacement in the Yemeni Red Sea*. US: AAPG.
- Hughes, G. W. a. G., and Johnson, R. S. (2005). Lithostratigraphy of the Red Sea region. *GeoArabia* 10, 49–126. doi:10.2113/geoarabia100349
- Ibrahim, E., Abd El-Motaal, E., Lashin, A., Alfaihi, H., Qaysi, S., and Kahal, A. (2021). Faulting intersections and magma-feeding zones in Tihamat-asir, Southeast red sea rift: Aeromagnetic and structural perspective. *Journal of African Earth Sciences* 173, 104044. doi:10.1016/j.jafrearsci.2020.104044
- Iding, M., and Ringrose, P. (2010). Evaluating the impact of fractures on the performance of the in Salah CO2 storage site. *International Journal of Greenhouse Gas Control* 4, 242–248. doi:10.1016/j.ijggc.2009.10.016
- Inama, R., Menegoni, N., and Perotti, C. (2020). Syndepositional fractures and architecture of the lastoni di formin carbonate platform: Insights from virtual outcrop models and field studies. *Marine and Petroleum Geology* 121, 104606. doi:10.1016/j.marpetgeo.2020.104606
- Jordá Bordehore, L., Riquelme, A., Cano, M., and Tomás, R. (2017). Comparing manual and remote sensing field discontinuity collection used in kinematic stability assessment of failed rock slopes. *International Journal of Rock Mechanics and Mining Sciences* 97, 24. doi:10.1016/j.ijrmmms.2017.06.004
- Kelmen, P. B., and Matter, J. (2008). *In situ* carbonation of peridotite for CO2 storage. *Proceedings of the National Academy of Sciences* 105, 17295–17300. doi:10.1073/pnas.0805794105
- Ligi, M., Bonatti, E., Bosworth, W., Cai, Y., Cipriani, A., Palmiotto, C., et al. (2018). Birth of an ocean in the Red Sea: Oceanic-type basaltic melt intrusions precede continental rapture. *Gondwana Research* 54, 150–160. doi:10.1016/j.gr.2017.11.002
- Madden, G. T., Schmidt, D. L., and Whitmore, F. C. (1983). *Mastritherium (artiodactyla, anthracoheriidae) from wadi sabya, southwestern Saudi Arabia: An earliest Miocene age for continental rift-valley volcanic deposits of the Red Sea margin*. Saudi arabia: Ministry of Petroleum and Mineral Resources, Deputy Ministry for Mineral.
- Marieni, C., Voigt, M., Clark, D. E., Gislason, S. R., and Oelkers, E. H. (2021). Mineralization potential of water-dissolved CO2 and H2S injected into basalts as function of temperature: Freshwater versus Seawater. *International Journal of Greenhouse Gas Control* 109, 103357. doi:10.1016/j.ijggc.2021.103357
- Matter, J., Stute, M., Snaebjörnsdóttir, S. Ó., Oelkers, E., Gislason, S., Aradóttir, E., et al. (2016). Rapid carbon mineralization for permanent disposal of anthropogenic carbon dioxide emissions. *Science* 352, 1312–1314. doi:10.1126/science.aad8132
- Mcdermott, C., Lonergan, L., Collier, J. S., Mcdermott, K. G., and Bellingham, P. (2018). Characterization of seaward-dipping reflectors along the South American Atlantic margin and implications for continental breakup. *Tectonics* 37, 3303–3327. doi:10.1029/2017tc004923
- Mcgrail, B. P., Spane, F. A., Amonette, J. E., Thompson, C. R., and Brown, C. F. (2014). Injection and monitoring at the Wallula basalt pilot project. *Energy Procedia* 63, 2939–2948. doi:10.1016/j.egypro.2014.11.316
- Mège, D., Purcell, P. G., Bézous, A., and Jourdan, F. (2016). *The ogaden dyke swarm: Red Sea rifting continued in the Somalia plate?* Beijing: Acta Geologica Sinica 56. English Edition.
- Menegoni, N., Giordan, D., and Perotti, C. (2020). Reliability and uncertainties of the analysis of an unstable rock slope performed on RPAS digital outcrop models: The case of the gallivaggio landslide (Western Alps, Italy). *Remote Sensing* 12, 1635. doi:10.3390/rs12101635
- Menegoni, N., Giordan, D., Perotti, C., and Tannant, D. D. (2019). Detection and geometric characterization of rock mass discontinuities using a 3D high-resolution digital outcrop model generated from RPAS imagery – ormea rock slope, Italy. *Italy. Engineering geology* 252, 145–163. doi:10.1016/j.enggeo.2019.02.028
- Menegoni, N., Meisina, C., Perotti, C., and Crozi, M. (2018). Analysis by UAV digital photogrammetry of folds and related fractures in the monte antola flysch formation (ponte organasco, Italy). *Geosciences* 8, 299. doi:10.3390/geosciences8080299
- Nex, F., and Remondino, F. (2014). UAV for 3D mapping applications: A review. *Applied geomatics* 6, 1–15. doi:10.1007/s12518-013-0120-x
- Nyberg, B., Nixon, C. W., and Sanderson, D. J. (2018). NetworkGT: A GIS tool for geometric and topological analysis of two-dimensional fracture networks. *Geosphere* 14, 1618–1634. doi:10.1130/ges01595.1
- Oelkers, E., Arkadaskiy, S., Afifi, A., Hoteit, H., Richards, M., Fedorik, J., et al. (2022). The subsurface carbonation potential of basaltic rocks from the Jizan region of Southwest Saudi Arabia. *International Journal of Greenhouse Gas Control* 120, 103772. doi:10.1016/j.ijggc.2022.103772
- Olsson, W. A., Lorenz, J. C., and Cooper, S. P. (2004). A mechanical model for multiply-oriented conjugate deformation bands. *Journal of Structural Geology* 26, 325–338. doi:10.1016/s0191-8141(03)00101-9
- Pallister, J. S. (1987). Magmatic history of Red Sea rifting: Perspective from the central Saudi Arabian coastal plain. *Geological Society of America Bulletin* 98, 400–417. doi:10.1130/0016-7606(1987)98<400:mhorsk>2.0.co;2
- Pallister, J. S. (1986). *Red-Sea rift magmatism near Al lith, kingdom of Saudi Arabia*. US: US Department of the Interior, Geological Survey.
- Peacock, D., Nixon, C., Rotevatn, A., Sanderson, D., and Zuluaga, L. (2016). Glossary of fault and other fracture networks. *Journal of Structural Geology* 92, 12–29. doi:10.1016/j.jsg.2016.09.008
- Pollyea, R. (2015). *System response as a function of relative permeability in geologic CO2 sequestration*. Washington, DC: American Geophysical Union.
- Schmidt, D. L., Hadley, D. G., and Brown, G. F. (1983). *Middle tertiary continental rift and evolution of the Red Sea in southwestern Saudi Arabia*. US: US Geological Survey.
- Schmufft, E., and Hadley, S. (1983). *Kingdom of Saudi Arabia*. Reston, VA: Stratigraphy of the Miocene Baid formation, southern Red Sea coastal plain, Kingdom of Saudi Arabia. Available at: <https://pubs.usgs.gov/of/1985/0241/report.pdf>.
- Sebai, A., Zumbo, V., Féraud, G., Bertrand, H., Hussain, A., Giannerini, G., et al. (1991). 40Ar/39Ar dating of alkaline and tholeiitic magmatism of Saudi Arabia related to the early Red Sea rifting. *Earth and Planetary Science Letters* 104, 473–487. doi:10.1016/0012-821x(91)90223-5
- Smith, J. V. (1997). Initiation of convergent extension fracture vein arrays by displacement of discontinuous fault segments. *Journal of Structural Geology* 19, 1369–1373. doi:10.1016/s0191-8141(97)00054-0
- Snaebjörnsdóttir, S. Ó., Gislason, S. R., Galeczka, I. M., and Oelkers, E. H. (2018). Reaction path modelling of *in-situ* mineralisation of CO2 at the CarbFix site at Hellisheidi, SW-Iceland. *Geochimica et Cosmochimica Acta* 220, 348–366. doi:10.1016/j.gca.2017.09.053
- Snaebjörnsdóttir, S. Ó., Oelkers, E. H., Mesfin, K., Aradóttir, E. S., Dideriksen, K., Gunnarsson, I., et al. (2017). The chemistry and saturation states of subsurface fluids during the *in situ* mineralisation of CO2 and H2S at the CarbFix site in SW-Iceland. *International Journal of Greenhouse Gas Control* 58, 87–102. doi:10.1016/j.ijggc.2017.01.007
- Snaebjörnsdóttir, S. Ó., Sigfússon, B., Marieni, C., Goldberg, D., Gislason, S. R., and Oelkers, E. H. (2020). Carbon dioxide storage through mineral carbonation. *Nature Reviews Earth & Environment* 1, 90–102. doi:10.1038/s43017-019-0011-8
- Steinitz, G., Bartov, Y., and Hunziker, J. (1978). K-Ar age determinations of some miocene-pliocene basalts in Israel: Their significance to the tectonics of the rift valley. *Geological Magazine* 115, 329–340. doi:10.1017/s0016756800037341
- Stockli, D. F., and Bosworth, W. (2019). “Timing of extensional faulting along the magma-poor central and northern Red Sea rift margin—Transition from regional extension to necking along a hyperextended rifted margin,” in *Geological setting, palaeoenvironment and archaeology of the Red Sea* (Germany: Springer), 81–111.
- Tanner, P. G. (1989). The flexural-slip mechanism. *Journal of Structural Geology* 11, 635–655. doi:10.1016/0191-8141(89)90001-1
- Thiele, S. T., Grose, L., Samsu, A., Micklethwaite, S., Vollgger, S. A., and Cruden, A. R. (2017). Rapid, semi-automatic fracture and contact mapping for point clouds, images and geophysical data. *Solid Earth* 8, 1241–1253. doi:10.5194/se-8-1241-2017
- Torres, J. E. A. (2020). *The potential for CO2 disposal in western Saudi Arabia: The jizan group basalts*. Thuwal: King Abdullah University of Science and Technology.
- Tubbs, R. E., Jr, Fouda, H. G. A., Afifi, A. M., Raterman, N. S., Hughes, G. W., and Fadolkarem, Y. K. (2014). Midyan peninsula, northern Red Sea, Saudi Arabia: Seismic imaging and regional interpretation. *GeoArabia* 19, 165–184. doi:10.2113/geoarabia1903165
- Vilarrasa, V., Carrera, J., and Olivella, S. (2013). Hydromechanical characterization of CO2 injection sites. *International Journal of Greenhouse Gas Control* 19, 665–677. doi:10.1016/j.ijggc.2012.11.014
- Voggenreiter, W., Hötzl, H., and Jado, A. (1988). Red Sea related history of extension and magmatism in the jizan area (southwest Saudi Arabia): Indication for simple-shear during early Red Sea rifting. *Geologische Rundschau* 77, 257–274. doi:10.1007/bf01848688
- Watkins, H., Butler, R. W., Bond, C. E., and Healy, D. (2015). Influence of structural position on fracture networks in the Torridon Group, Achnashellach fold and thrust belt, NW Scotland. *Journal of Structural Geology* 74, 64–80. doi:10.1016/j.jsg.2015.03.001
- Wolfenden, E., Ebinger, C., Yirgu, G., Renne, P. R., and Kelley, S. P. (2005). Evolution of a volcanic rifted margin: Southern Red Sea, Ethiopia. *Geological Society of America Bulletin* 117, 846–864. doi:10.1130/b25516.1
- Zwaan, F., Corti, G., Sani, F., Keir, D., Muluneh, A. A., Illsley-Kemp, F., et al. (2020). Structural analysis of the western Afar margin, east africa: Evidence for multiphase rotational rifting. *Tectonics* 39, e2019TC006043. doi:10.1029/2019tc006043